Journal of Structural Geology 31 (2009) 222–236

Contents lists available at ScienceDirect

Journal of Structural Geology

journal homepage: www.elsevier.com/locate/jsg

3D Analysis of an Ordovician igneous ensemble: A complex magmatic structure hidden in a polydeformed allochthonous Variscan unit

Rubén Díez Fernández [a,*], José R. Martínez Catalán [a]

[a] Departamento de Geología, Universidad de Salamanca, Plaza de la Merced s/n, 37008 Salamanca, Spain

ARTICLE INFO

Article history:
Received 1 April 2008
Received in revised form
27 November 2008
Accepted 29 November 2008
Available online 13 December 2008

Keywords:
Ring dikes
Pluton geometry
Recumbent folds
Allochthonous complexes
Iberian Massif

ABSTRACT

The basal units of the allochthonous complexes of NW Iberia represent a fragment of the external edge of Gondwana subducted and subsequently exhumed during the Variscan collision. The structural analysis carried out in orthogneissic massifs of the southern part of one of these, the Malpica–Tui Unit, reveals the generation of recumbent folds and associated axial planar foliation during their exhumation. These folds nucleated in irregular igneous bodies that were initially deformed during the subduction event and show east to southeast vergence. Down-plunge projection of surface data and a series of regularly spaced cross-sections have been used to build 3D models of the two main bodies of orthogneiss, of calc-alkaline and peralkaline compositions respectively. The first is presently a lens-shaped body folded in a recumbent syncline, whereas the peralkaline gneiss, also affected by a train of asymmetric recumbent folds in the south, exhibits in the north a fold-like structure which is interpreted as inherited from its primary geometry, that of a ring dike pluton.

1. Introduction

Establishing the geometry of granitic plutons may provide clues about their emplacement mechanisms and tectonic setting. 3D geometries are usually obtained combining structural and AMS analyses with gravity and magnetic modelling. These techniques are applied successfully to the study of plutons either undeformed or deformed during their emplacement, that is, to syn- to post-kinematic granite massifs (Bouchez et al., 1990; Yenes et al., 1999; Simancas et al., 2000; Aranguren et al., 2003; Neves et al., 2003; Talbot et al., 2004, 2005).

The original shape of strongly deformed granitic gneisses is much more difficult to establish. Deformation of igneous bodies with contrasted viscosity inside a shear zone can include rotation, shortening, flattening, and stretching, and can be accompanied by folding, boudinage, and the development of relative discrete shear zones from crystal to crustal scale. The whole gneissification of kilometre-scale granitic massifs implies deep changes in their geometry that often obscures what kind of igneous intrusion they represent. The reconstruction of the original shapes is usually impossible, as it would need a detailed knowledge of the finite strain for the whole volume of the bodies to carry out a three dimensional restoration.

However, even when strongly flattened and/or stretched, the chronological order of emplacement of different plutons can be established using cross-cutting relationships, and hints on their primary geometry can arise from their deformed shapes. Initially rounded, equidimensional plutons may become folded, specially when deformation is polyphasic, which adds complexity to the correct interpretation of the plutons. In that case, a structural study using basic geometrical techniques can be applied to identify fold geometry and separate folds from primary igneous geometries. Linkage between primary igneous geometries and room available during emplacement allows certain shapes of igneous bodies to be related to particular stress regimes, and ultimately to specific geodynamic contexts. As there is also a connection between magmatic associations and geodynamic context (Pitcher, 1993; Barbarin, 1999), magma type can be used as a helpful guide to envisage the original igneous structure at the light of these relations.

This is the case presented here, where two orthogneisses of different composition are strongly deformed and folded, and where their folded geometries and mutual relationships, combined with the peculiar composition of one of the massifs, permits the original shape of both massifs to be envisaged.

2. Geological setting

The allochthonous complexes of NW Iberia represent a nappe stack where three main groups of allochthonous units have been

* Corresponding author. Tel.: +34 923 294488; fax: +34 923 294514.
E-mail addresses: georuben@usal.es (R. Díez Fernández), jrmc@usal.es (J.R. Martínez Catalán).

0191-8141/$ – see front matter © 2008 Elsevier Ltd. All rights reserved.
doi:10.1016/j.jsg.2008.11.017

distinguished (Martínez Catalán et al., 2007). The upper units are pieces of a Cambro-Ordovician ensialic island arc (Andonaegui et al., 2002; Santos et al., 2002; Abati et al., 2003), the middle units are ophiolitic, and represent the suture of the Rheic Ocean (Díaz García et al., 1999; Pin et al., 2002, 2006; Arenas et al., 2007; Sánchez Martínez et al., 2007), and the basal units derive from distal parts of the Gondwanan continental margin. The basal units experienced extension and rift-related magmatism during the Ordovician (Ribeiro and Floor, 1987; Pin et al., 1992), subduction at the beginning of the Variscan collision (Van Calsteren et al., 1979; Santos Zalduegui et al., 1995; Rodríguez et al., 2003) and exhumation driven by crustal-scale thrusting accompanied by recumbent folding, and tectonic denudation during the Variscan orogeny (Gil Ibarguchi and Ortega Gironés, 1985; Arenas et al., 1995; Martínez Catalán et al., 1996, 1997; Rubio Pascual et al., 2002).

This study is centred in the southern part of the Malpica–Tui Unit, one of the basal allochthonous units that crops out in the western part of Galicia, in NW Iberia (Fig. 1). The Malpica–Tui Unit shows the characteristics of a thinned continental crust, and consists of a thick terrigenous pile of sediments intruded by a bimodal suite of granitic and basic magmas of Ordovician age deformed during the Variscan orogeny (Van Calsteren et al., 1979; García Garzón et al., 1981; Santos Zalduegui et al., 1995). The granitic rocks include felsic and biotitic gneisses with calc-alkaline affinities (tonalites, granodiorites and high-K granites), a mildly alkaline association composed of metaluminous alkali-feldspar quartz-syenites and granites, peraluminous alkali-feldspar granites and peralkaline granites (Rodríguez Aller, 2005). The protoliths of the alkaline and peralkaline gneisses seem to be younger than the calc-alkaline gneisses because they lack the widespread basic intrusions included in the felsic and biotite gneisses and in the metasediments.

One of the main features of the Malpica–Tui Unit and other units occupying the lower position of the allochthonous tectonic pile is the record of an early Variscan high-pressure metamorphic event (Gil Ibarguchi and Ortega Gironés, 1985; Rodríguez et al., 2003) related to subduction with a west-directed component. Subduction was followed by exhumation and emplacement toward the east, over their relative autochthon which represents relatively inner parts of Gondwanan continental margin (Martínez Catalán et al., 1996, 1997; Rubio Pascual et al., 2002).

3. Variscan deformation events

Three main phases of deformation can be recognized in the Malpica–Tui Unit. The first (D_1) is only identified as an internal fabric ($S_i = S_1$) included in porphyroblasts (Fig. 2). But it is important because that fabric is the one associated to the high-pressure metamorphic event. The second phase (D_2) is associated to the main tectonic foliation (S_2), and related to recumbent folding and the exhumation of the unit by thrusting. The third deformation phase (D_3) gave rise to upright folds that bent the main foliation and produced fold-interference patterns.

3.1. Relicts of early-Variscan subduction (D_1)

Aligned internal fabrics (S_i) in blasts of albite in metasediments and of plagioclase in amphibolites, plus the presence of S_2 crenulation cleavage in the metasediments (Fig. 3a), prove the existence of an initial phase of deformation (D_1) strong enough to generate a planar tectonic fabric (S_1) and consequently to modify the original shape of the igneous bodies.

In the metasediments, the stable mineral assemblage consists of quartz, white mica, garnet, and rutile preserved in S_2 crenulated microlithons (Fig. 3b) and in the core of albite porphyroblasts (Fig. 3c). Stable growth of garnet without biotite, the presence of rounded reabsorbed turbid garnets and the atoll-like texture of those not included in the porphyroblasts support initial conditions of high pressure and low to medium temperature (Higashino, 1990; Otsuki and Banno, 1990; Takasu and Dallmeyer, 1990). These are in accordance with similar conditions established in other basal units of NW Iberia (Munhá et al., 1984; Schermerhorn and Kotsch, 1984; Gil Ibarguchi and Ortega Gironés, 1985; Díaz García, 1990; Arenas et al., 1995; Martínez Catalán et al., 1996; Rodríguez Aller, 2005). The assemblage in the metasediments is compatible with the inclusions of garnet, amphibole, rutile, chlorite, epidote and quartz inside the plagioclase of amphibolites, although this is not a characteristic high-pressure association in the metabasites. Even if there are no eclogite or blueschist facies indicators in the southern part of the Malpica–Tui Unit, small-sized garnet and rutile included in the porphyroblasts of plagioclase and absent in the matrix are a typical feature of retrogressed high-pressure metabasites in the northern parts of the unit (Gil Ibarguchi and Ortega Gironés, 1985).

Because of the lack of quantitative data, a conservative estimation of the pressure has been made based on the absence of eclogite assemblages in the metabasites and the scarce development of garnet in the metasediments compared with other related basal allochthonous units in NW Iberia (Arenas et al., 1995). Accordingly, we suggest a minimum pressure of 1 GPa during D_1, in a context of continental subduction. This interpretation confers an exhumative character to the second deformation phase (D_2), which moved the unit from these burial conditions to the amphibolite facies domain, and which was followed by further depressurization and heating during D_3.

3.2. The regional fabrics (D_2)

This phase is responsible of large recumbent folds affecting the orthogneisses and of the regional foliation (S_2) and lineation (L_2). The main foliation in the metasediments appears as a schistosity defined by statistically oriented quartz, biotite and white mica, subparallel or oblique to a compositional layering (S_0, Fig. 3d), and including albite porphyroblasts. When oblique to S_0, an intersection lineation can be observed.

The granitic orthogneisses include augen, planar, linear, planolinear and mylonitic varieties, pointing to heterogeneities in the deformation and perhaps to original textural and mineralogical heterogeneities in the igneous rocks. Index minerals and geochemical and textural features make it possible to map different gneissic bodies which may represent either single or composite related intrusions. Three main kinds of intrusive magmas can be distinguished: calc-alkaline, alkaline and peralkaline (Floor, 1966; Rodríguez Aller, 2005). All of them show a gneissic foliation and a mineral lineation formed by an alternation and alignment of quartz-feldspathic bands and different ferromagnesian minerals depending on the composition. These index and other secondary minerals are oriented and aligned, individually or in aggregates, parallel to the main foliation and lineation.

The largest massif in the study area is a biotite orthogneiss (Fig. 4) with calk-alkaline affinity containing biotite and lesser amounts of green amphibole (hornblende) as ferromagnesian index minerals (Fig. 3e). For the alkaline orthogneiss, cropping out in the southern part of the study area (Fig. 4), the index minerals are biotite and an alkaline green amphibole (hastingsite), both occurring generally in the same proportion but sometimes with one of them dominating among the ferromagnesian phases (Fig. 3f).

The peralkaline orthogneisses include riebeckite (blue amphibole) and/or aegirine (green pyroxene) as main index minerals, whereas astrophyllite occurs sometimes as a minor constituent of the rock (Fig. 3g). Occasionally, these gneisses crop out related with

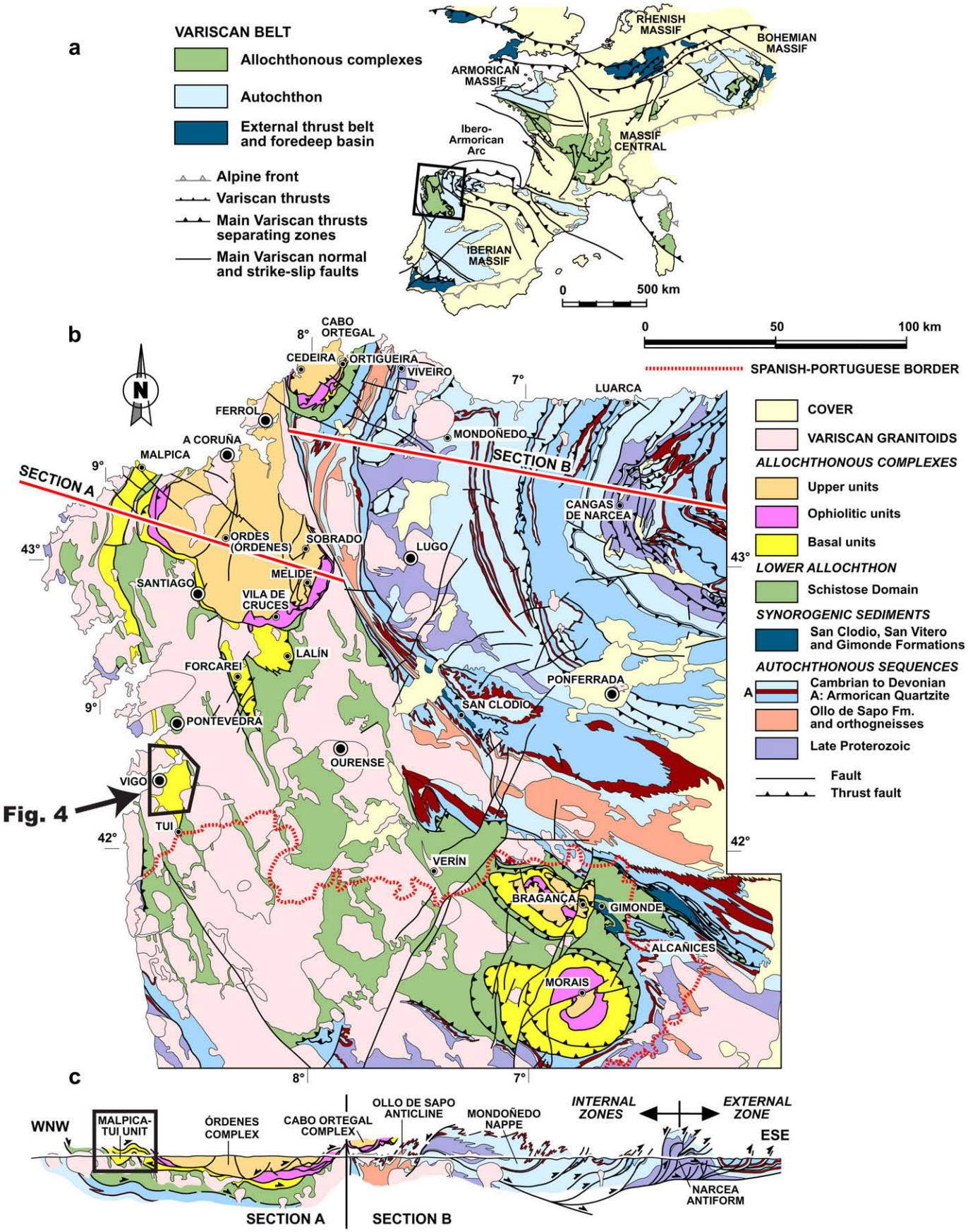

Fig. 1. Situation of the study area in the Variscan belt of Europe (a), and in a geological map (b) and cross-section (c) of NW Iberia (after Martínez Catalán et al., 2008).

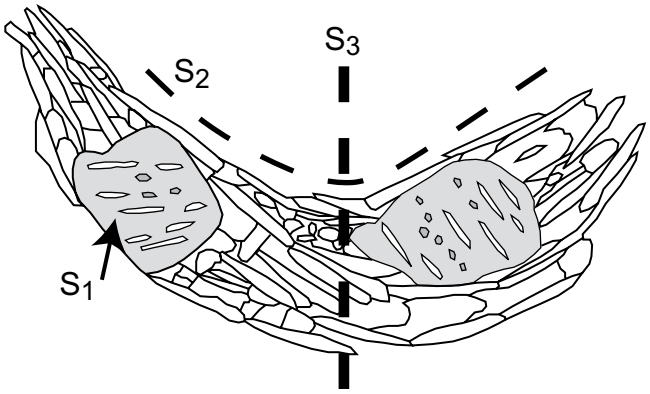

Fig. 2. Textural sketch of the relationships between the tectonic fabrics developed in a metasediment that recorded the main phases of deformation recognizable in the Malpica–Tui Unit.

biotite (annite?) gneisses in the same igneous body (Floor, 1966). This kind of biotite orthogneiss differs from the previously described biotite gneiss (calk-alkaline affinity) in its textural features (it resembles the peralkaline gneiss), the composition of the biotite (annite?) and the presence of albite porphyroclasts (less common in the biotite orthogneiss).

Basic intrusions in the metasediments and in the biotite orthogneiss crop out as meter-scale amphibolite boudins surrounded by the S_2 fabric (Fig. 3h). The hornblende–plagioclase stable mineral assemblage in the basic rocks and the mica–quartz–albite assemblage in the metasediments point to medium to low pressure (0.5–0.6 GPa) and medium temperature (<550 °C) amphibolite facies conditions during D_2.

3.3. Late upright folding (D_3)

The main tectonic foliation appears bent by open folds that are progressively tighter to the north and show vertical axial surfaces. North-plunging axes in the southern part of the study area and south-plunging axes in the north configure a structural basin with a dome at its core limited by a ring synform (Fig. 4).

D_3 fold axes are parallel to the limits of the Malpica–Tui Unit and plunge following the dip of the limbs of the structural basin and the dome, as does the mineral lineation in the gneisses (Fig. 4). This fact suggests that both the main foliation and the lineation in the

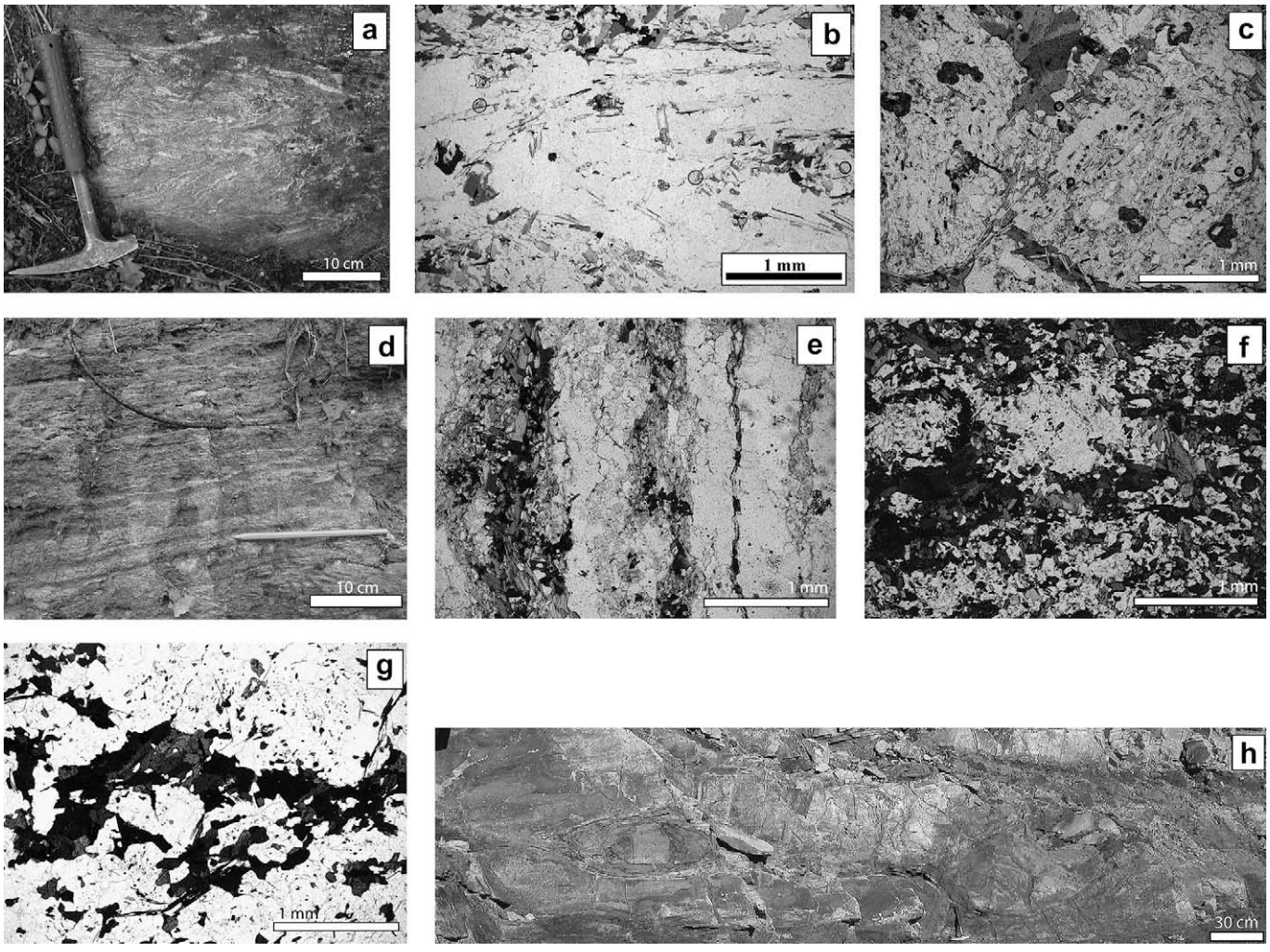

Fig. 3. (a) D_2 microfolds in albite-bearing schists. (b) Thin section of an albite-bearing schist showing a folded schistosity (S_1), not included in albite porphyroblasts, marked by atoll-like garnet, quartz, rutile and white mica partly retrogressed to biotite at its rims. (c) Aligned high-pressure microinclusions (S_1) of garnet, rutile, quartz and white mica in albite porphyroblasts. (d) S_2 schistosity (parallel to the pencil) oblique to compositional layering in albite-bearing schists. (e) Microphotograph showing the S_2 foliation in the biotite orthogneiss. (f) Microscopic aspect of the S_2 foliation in the alkaline orthogneiss. (g) S_2 foliation in the peralkaline orthogneiss. (h) Amphibolite boudins included in the biotite orthogneiss.

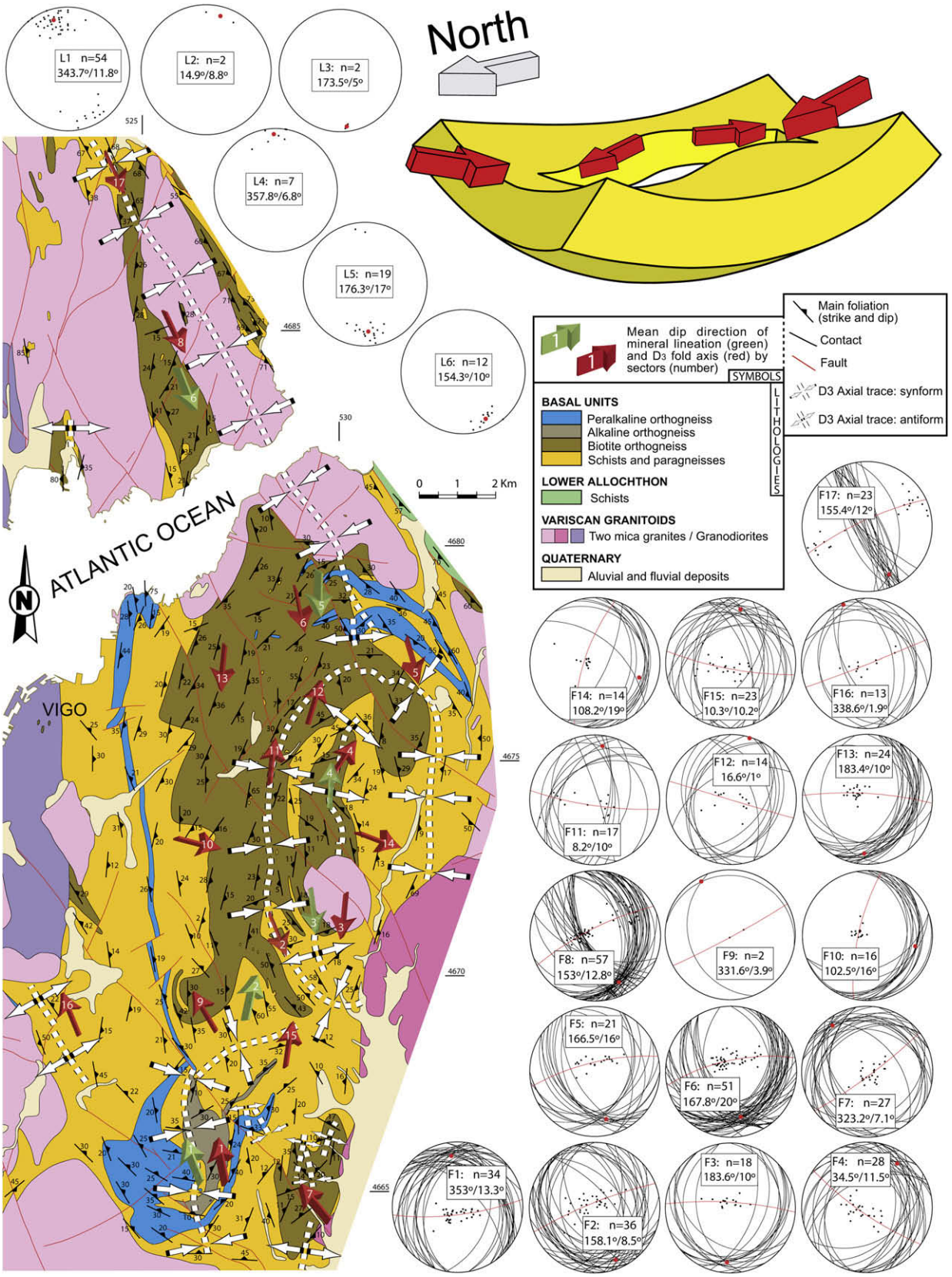

Fig. 4. Geological map of the southern part of the Malpica–Tui Unit (left) with a simple model of the D_3 structure (upper right corner), deduced from the structural analysis (stereographic plots of the main foliation (S_2) by sectors; right). The plots include the planes (large circles), the pole to the planes (dots), the cylindrical best fit (red large circles) and the orientation of D_3 fold axes obtained (red dots). The plots in the upper left corner show the mean direction of the mineral lineation plotted by sectors. The foliation symbols represent the mean strike and dip direction of several measures in the area. The arrows represent the mean direction of D_3 fold axes (red) or mineral lineation (green). The sectors used for the stereographic plots are indicated by the number inside the arrows. Map coordinates are UTM.

orthogneisses are folded by D_3 and should be related to previous deformation events.

Simultaneous with D_3, disorganized mineral recrystallization occurred, as sillimanite, poikiloblastic andalusite and cordierite grew including the main tectonic foliation (S_2). Locally, in the western side of the ring syncline, an S_3 cleavage developed as a nearly-vertical planar fabric in the gneisses parallel to the axial surface of D_3 folds. Considering pressures of 0.3–0.4 GPa obtained for the crystallization of late muscovites and amphiboles by Montero (1993), a minimum temperature of 500 °C can be estimated from the growth of andalusite (Holdaway, 1971).

The open character of D_3 folds in the study area and the common lack of an associated cleavage cast doubts on their relationship with a contractional event. The late, low-pressure metamorphic evolution of the area, together with what is known in surrounding areas (Martínez Catalán et al., 2007) suggest that the open folds are the product of dome and basin development linked to late Variscan extensional collapse. In particular, the small elongated antiform developed in the core of an open synform is spatially related to the growth of cordierite porphyroblasts in metasediments, and is interpreted as overlying a granitic or magmatic dome of smaller size than the common regional gneiss domes. However, the dome and basin structure was overprinted by large strike-slip shear zones (Iglesias Ponce de León and Choukroune, 1980), mostly developed after the gravitational collapse of the orogen. They are responsible for tightening of the previous, extension-related open folds.

4. Geometry of the recumbent folds

4.1. Deformation of igneous bodies: Generalities

Intrusive igneous bodies are geometrically characterized by having variable morphologies and irregular contours, determined by the stress regime, rheological properties and viscosity contrasts with the host rocks and by the room potentially available during their emplacement (Fig. 5a).

The unpredictability of their original shape hinders the macrostructural analysis of intrusive bodies, whereas the microstructures, mainly fabrics, yield the evidence of deformation and at least a hint about its intensity. In the case of the Malpica–Tui Unit, the first deformation phase (D_1) is characterized by an initial foliation (S_1) generalized to the scale of the unit, that evidences flattening and permits the assumption of flat morphologies after deformation. Roughly equidimensional massifs (Fig. 5b) deformed more or less homogeneously would transform into lens-shaped bodies ranging between the oblate and prolate types depending on their original shape and the superimposed finite strain. As S_1 is coeval with the first, high-pressure metamorphic event, it is viewed as related to subduction, and a strong component of simple shear can be envisaged. This would imply the development of a linear fabric accompanying the foliation, and an elongated-lens shape for an originally spherical igneous body.

Whereas an equidimensional body would not be folded, a tabular or lens-shaped body could be. The incomplete deletion of primary irregularities and the generation of new ones by boudinage and/or folding during syn-D_1 shearing and flattening might propitiate the nucleation, propagation and amplification of folds starting from these mechanical instabilities during the subsequent deformation events in rocks that exhibit a viscosity or competence contrast (Cobbold, 1975), such as the orthogneisses and their metasedimentary host (Fig. 5c).

From the point of view of deformation mechanisms, both blueschist and eclogite facies metamorphism in the Malpica–Tui Unit reached 500 °C during D_1 subduction (Gil Ibarguchi and Ortega Gironés, 1985; Rodríguez et al., 2003; Rodríguez Aller, 2005). These temperatures where maintained during a significant part of D_2 exhumation, as constrained by S_2 mineral assemblages indicating amphibolite facies conditions. Under such temperatures, quartz-feldspathic rocks would exhibit a fully ductile behaviour (Tullis and Yund, 1985; Bozkurt and Park, 1997).

4.2. Recumbent folds in the peralkaline orthogneiss: The down-plunge section

The first hint of the possible existence of recumbent folds came from the map pattern of the peralkaline orthogneiss occurring in the southern part of the study area (Fig. 4 and Floor, 1966). There, the roughly tabular body shows considerably widening and depicts

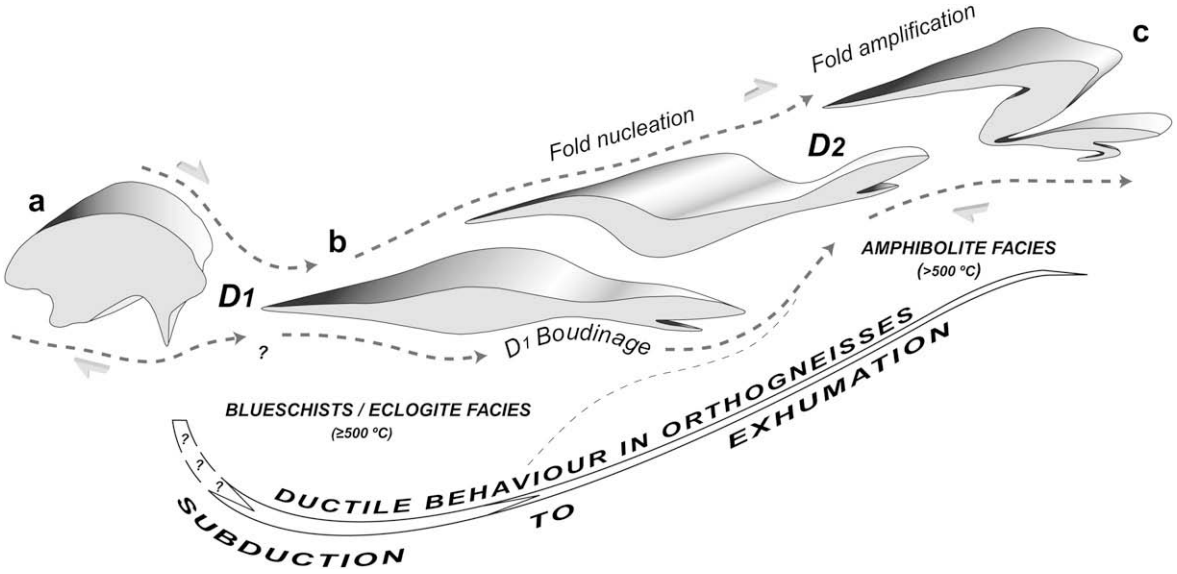

Fig. 5. Idealized evolution of an irregular intrusive igneous body (a) affected by an initial deformation event (D_1), which transforms it into an irregular lens-shaped orthogneiss (b) and is subsequently folded (c) during a later deformation phase (D_2). Both deformations have a large component of simple shear and took place under blueschist or eclogite facies and amphibolite facies conditions respectively, at temperatures high enough to guarantee ductile deformation behaviour of the orthogneisses.

an irregular shape reminiscent of either large-scale boudinage or folding. The fact that the main foliation (S_2) is sometimes parallel, sometimes oblique, even perpendicular, to the limits of the orthogneisses, suggests that we are dealing with folds and that the zones of higher obliquity correspond to the hinge zones of such folds.

A D_3 synform occurs also in the southern part of the study area, so that if D_2 recumbent folds exist the map depicts a fold interference pattern. To test this assumption, a detailed structural analysis was carried out, and a down-plunge section (Mackin, 1950) was built normal to the calculated fold axis, to obtain the geometry of the folds. In doing that, we must treat the structures as cylindrical, but in zones with several fold generations, every fold family must be identified and its fold axis and axial surface characterized, in order to get the best possible image of each family of folds.

The main tectonic foliation (S_2) in the southern part of the study area is folded in an upright synformal structure with north-plunging axis (353°/13°) (Fig. 4, stereographic plot F1). The hypothetical recumbent folds occur only at the western limb of the synform, so that only this limb will be projected down plunge along the mean axis deduced for the recumbent folds to show their geometry. The mean axis has been obtained from direct measurements of minor D_2 folds in metasediments and amphibolites (Fig. 3a), from the intersection between the sedimentary layering and S_2 (Fig. 3d), and from the intersection between the orthogneiss/metasediment contacts and S_2 in the assumed hinge zone (Fig. 6). Its orientation is 35°/17°.

The down-plunge section (Fig. 7) shows a train of recumbent folds with dextral asymmetry, thick hinges and thin limbs, variable amplitude and wavelength, and interlimb angles ranging from 76° to 18°, which points to inhomogeneous flattening. The projection of the main foliation (S_2) on the down-plunge section demonstrates that S_2 is an axial planar foliation of the recumbent folds as suspected (Fig. 8a). Its parallelism with the axial surfaces and refraction in the hinge zones are typical of folded layers exhibiting competence contrasts (Ramsay and Huber, 1987, pp. 461–466).

Dip isogons and their projection into the $t'_\alpha - \alpha$ graphic of Ramsay (1967) show that folds are dominantly similar (class 2 of Ramsay, 1967), which points to a strong superimposed flattening (Fig. 8b).

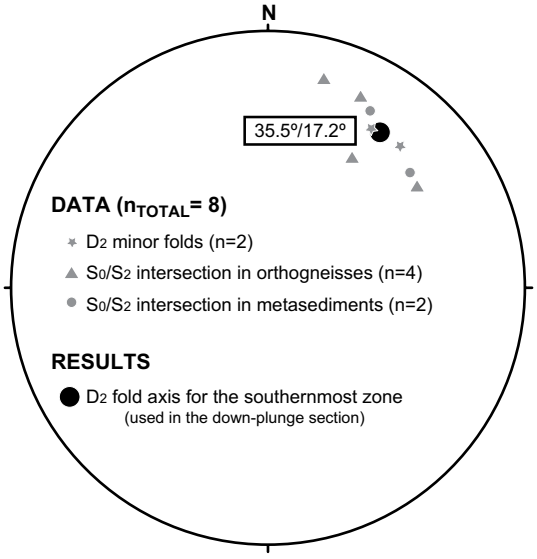

Fig. 6. Calculation of D_2 fold axis orientation as the mean vector of structurally significant linear elements in the southern part of the study area. This fold axis was used to build up the down-plunge section of Fig. 7.

Assuming that the refracted S_2 foliation at fold hinges shares a common straight line, the mean vector of the intersections of the refracted foliations (Fig. 8a) can be used to validate the orientation of D_2 fold axes used in the down-plunge section. Contours in Fig. 8a show a considerable dispersion, which may arise from the fact that both D_2 folds and their axial planar foliation are weakly refolded. Reorientation of S_2 could have increased the non-coaxiality of D_2 folds and, more importantly, distorted the mutual intersections among the different orientations of the main foliation. Nevertheless, the two maxima obtained in two areas of the recumbent structure (Fig. 8a) do not differ very much from the mean orientation for D_2 fold axes obtained from independent criteria (35°/17°; Fig. 6).

The mean orientation for D_2 fold axes reveals a remarkable obliquity (50°) with the mean vector of the mineral lineation (344°/12°; Fig. 4, stereographic plot L1) associated with S_2 in the southern area (Fig. 9). This suggests that L_2 is a stretching lineation and not an intersection lineation. This interpretation is in accordance with the preferred statistical orientation of minerals and mineral aggregates derived from the recrystallization of pre-existing grains and with the elongation exhibited by the gneiss massifs, as described below. However, as D_2 was preceded by a ductile deformation event, and the orthogneisses may register in one single fabric a complex strain history (Watterson, 1968; Coward, 1972), L_2 could represent the superposition of D_1 and D_2 deformation events.

The map pattern of the peralkaline gneiss in the southern area shows a hook-type interference between D_2 and D_3. However, using Ramsay's classification (Ramsay, 1967), the interference is of type 2, that is, of the mushroom kind, because the angle between D_2 and D_3 axes is higher than 20°, the limit proposed by the author between interference patterns of types 2 and 3. As the peralkaline orthogneiss pinches out and disappears to the NE before the D_2 hinges have the opportunity to emerge in the eastern limb of the D_3 synform, a mushroom-type map interference should not be expected.

4.3. Recumbent folds in the biotite orthogneiss

Once the major D_3 folds have been identified, we have analyzed the cartographic pattern of the biotite gneiss contacts in relation to the attitude of S_2 foliation, which has been demonstrated to be axial planar to D_2 recumbent folds in the peralkaline orthogneiss. Our study shows that when the contacts are curved, two kinds of relationship with S_2 can be observed. When S_2 is strongly oblique to normal to the contact, we interpret it as the hinge zone of a recumbent fold, whereas those inflexions whose outlines are parallel to S_2 are interpreted as D_3 hinge zones. The analysis demonstrates the existence of a D_2 recumbent fold whose hinge zone can be followed from south to north cropping out in both limbs of the D_3 structural basin with a small dome at its centre (zones 1–4 in Fig. 10a). In the absence of way-up criteria, this recumbent fold (Fig. 10b) could be either an anticline or a syncline. However, assuming that the regional vergence is to the east, as for the rest of large recumbent folds in NW Iberia (Martínez Catalán et al., 1996, 2007), it will be interpreted as a syncline. This syncline provides a cartographical checkup of D_2 folds axes orientation, which varies from NE–SW in the south to NNE–SSW in the north (Fig. 10c).

The central part of the western contact of the biotite orthogneiss depicts a zig-zag pattern in zones 5– 7 of Fig. 10a, corresponding to a SE-verging train of recumbent folds like the ones deduced from the down-plunge section for the peralkaline orthogneiss to the south (Fig. 7). Moreover, whereas the fold hinge in 5 reappears in 6, several fold hinges around zones 6 and 7 do not continue to the south (zone 8, Fig. 10a). So, the analysis of this fold train suggests

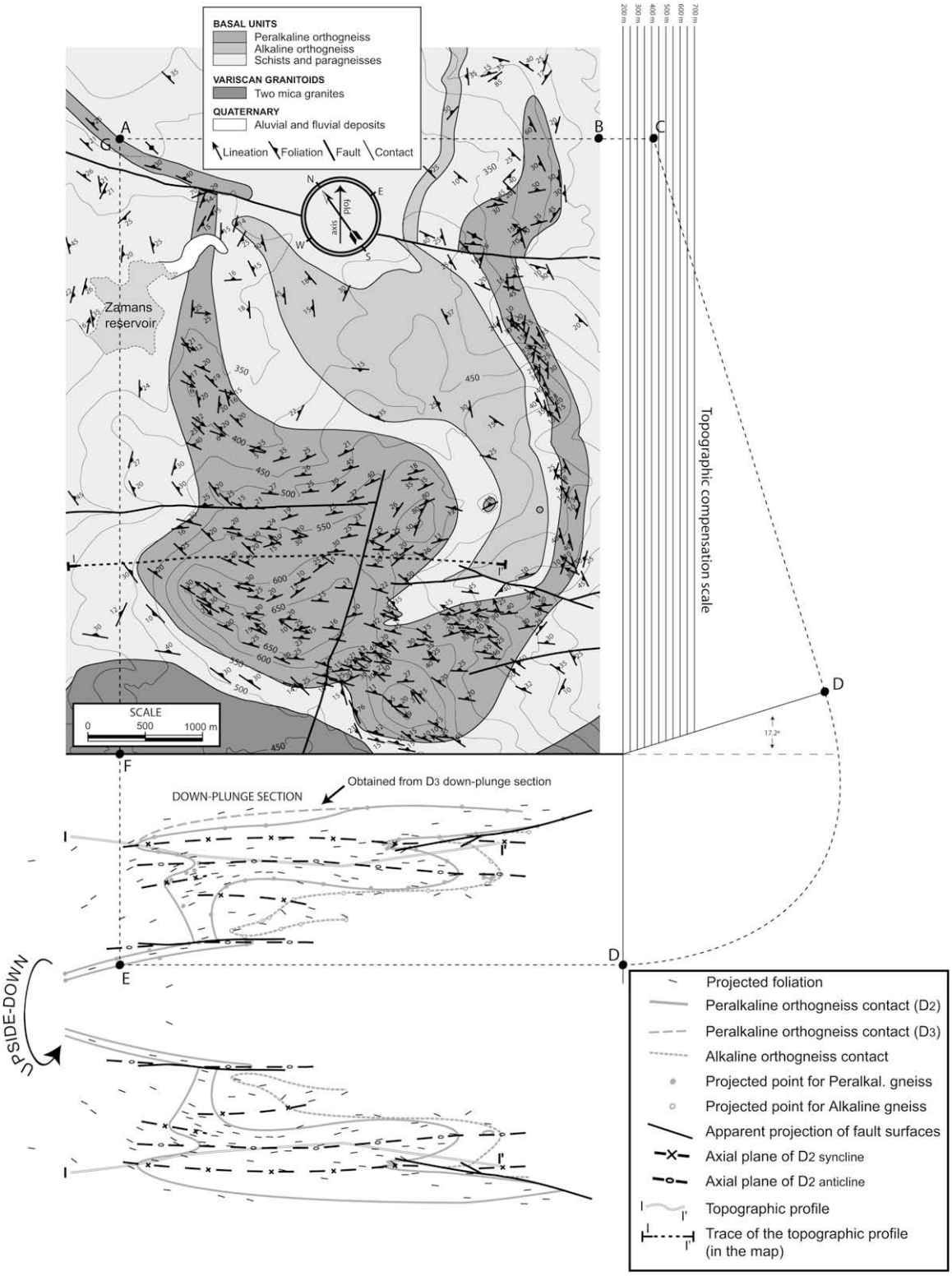

Fig. 7. Down-plunge section of peralkaline and alkaline orthogneisses built to obtain the geometry of D_2 recumbent folds in the southernmost part of the study area. The section includes the projection of the contacts of each unit in the western limb of the D_3 synform, built linking points projected from the contacts. The lower limb of the peralkaline orthogneiss (thick dashed line) has been obtained from a down-plunge section (not included) normal to the D_3 fold axis (plot F1, Fig. 4), because its geometry is related to the upright folds. The final structure of the peralkaline orthogneiss results from the fusion of the D_2 and D_3 down-plunge sections. The projection of the S_2 foliation and faults (the latter without structural meaning in the section) are included. The workflow from A (map point to be projected) to E (projection of the point) is displayed as an example of the procedure followed. The position of a point in the section is given by the intersection of a line parallel to the mean D_2 fold axis (35°/17°) passing by A, with the surface perpendicular to this line, after correcting for the effect of the topography (topographic compensation scale). Because of the geometrical technique used, the section is upside-down and must be rotated to view the D_2–D_3 structure in a normal position (bottom).

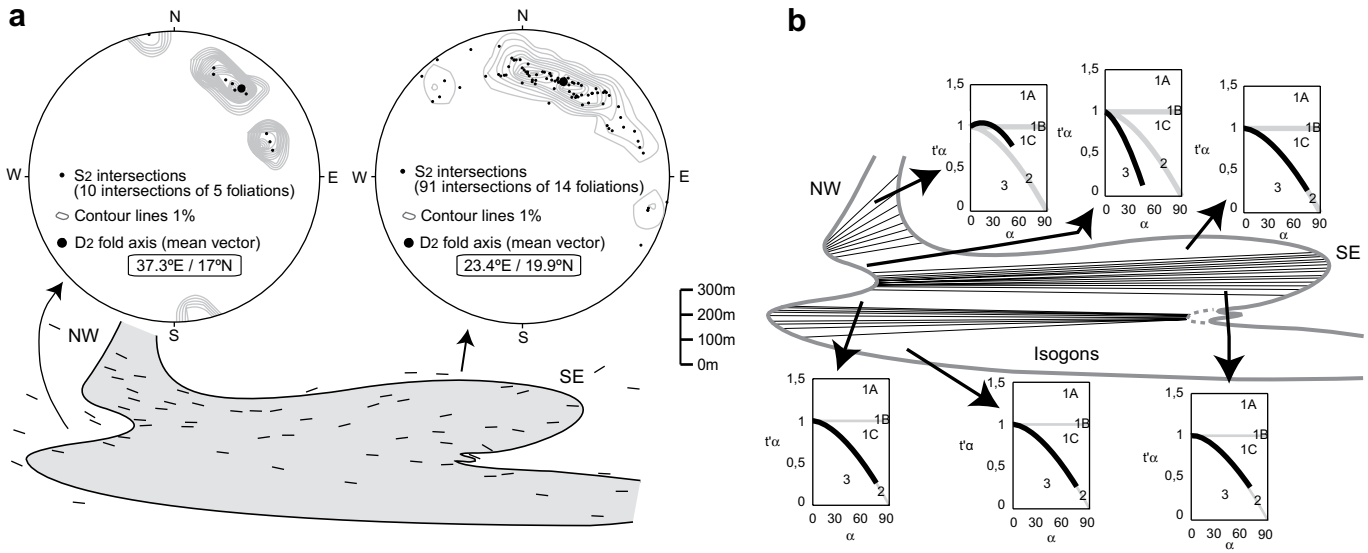

Fig. 8. (a) Stereographic plots of S_2 in two of the fold hinge zones. D_2 fold axes are obtained as the mean vector of the mutual intersections of the refracted foliations, which are assumed to be zonal. (b) Dip isogons for the D_2 limbs and their projection into the $t'_\alpha - \alpha$ graphic of Ramsay (1967) plotted using the software of Vacas Peña (2001). The arrows link each limb with the corresponding graphic.

thinning of the deformed igneous body towards the south. The outcropping of the same fold hinge twice (5 and 6, Fig. 10a) as a consequence of late, open folding, indicates a N–S attitude for these D_2 folds axes. This deviation in the orientation in relation with previously described fold hinges is explained by a pre-D_2 obliquity of the folded surfaces, which can be interpreted in terms of a lenticular shape of the biotite orthogneiss.

These features reveal three-dimensional variations in thickness along and across the biotite orthogneiss, which can be explained by the inherited shape of the protolith, modified by flattening and stretching during D_1 and D_2. The thin band at its southern contact (8, Fig. 10a) may be interpreted as a modified original igneous protuberance.

With these premises, eleven regularly spaced sections normal to the NE axes orientation of D_2 folds were made across both gneiss bodies (Fig. 10b). They show a tight syncline for the biotite orthogneiss, affecting an irregular pluton elongated in the N–S direction. At the upper fold limb, the pluton pinches out and ends (9 in Fig. 10a), supporting the interpretation of its shape being lenticular. Towards the north, the hinge zone of the syncline hosts a strip of peralkaline and related rocks that seem to be folded in what looks like a recumbent fold of the opposite kind, that is, an anticline (to the east of 4 in Fig. 10a). The cross-section K shows the geometry of both, peralkaline and biotite orthogneisses, depicting the paradoxical image of a fold that is either a syncline or an anticline depending on the pluton affected.

4.4. 3D rendering of the folded plutons

Fig. 10d and e show two different 3D perspectives of the main biotite orthogneiss body made by tracing a surface envelope joining the structurally correlated and regularly spaced cross-sections of Fig. 10b with the aid of CAD software. The model shows a major recumbent syncline with minor folds at the hinge zone, affecting a massif elongated in the N–S direction. The deformed pluton ends towards the south and thickens towards the north, suggesting a pre-D_2 lenticular shape. The structural basin with a dome at its centre, forming a ring syncline around, can also be appreciated in both views.

The interpretation of the peralkaline orthogneiss as a single body is depicted in Fig. 11a, which includes the tight fold-like structure in the northeast (1), the small isolated masses cropping out to the west of it (2), the elongated band ending with an inflexion in the northwest (3), and the recumbent train of folds in the south (4). Fig. 11b–d show 3D perspective views of the pluton. Its shape in the northern part might represent either a sheath fold with a NE–SW apical direction, or an incomplete ring dike flattened and stretched.

No 3D model has been made for the alkaline orthogneiss because its integration in the whole 3D model (see below) would have hidden the train of recumbent folds in the lower side of the peralkaline orthogneiss. Moreover, the absence of outcrops of the alkaline gneiss towards the north, even when the plunge of D_3 fold axes changes from north to south in the area, suggests that this

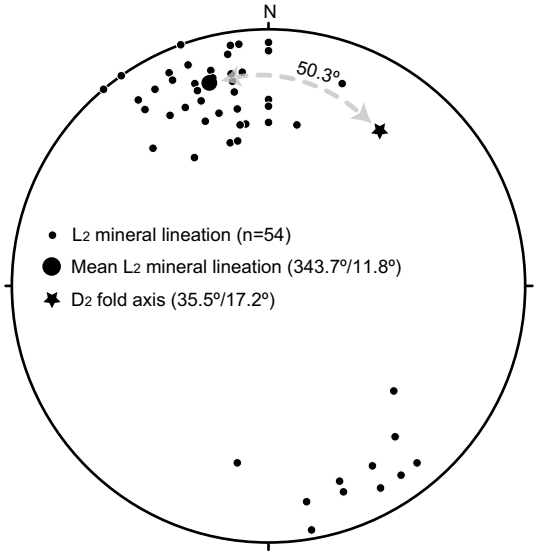

Fig. 9. Angular relationship between the mean vector of the mineral lineation (L_2) and D_2 fold axes.

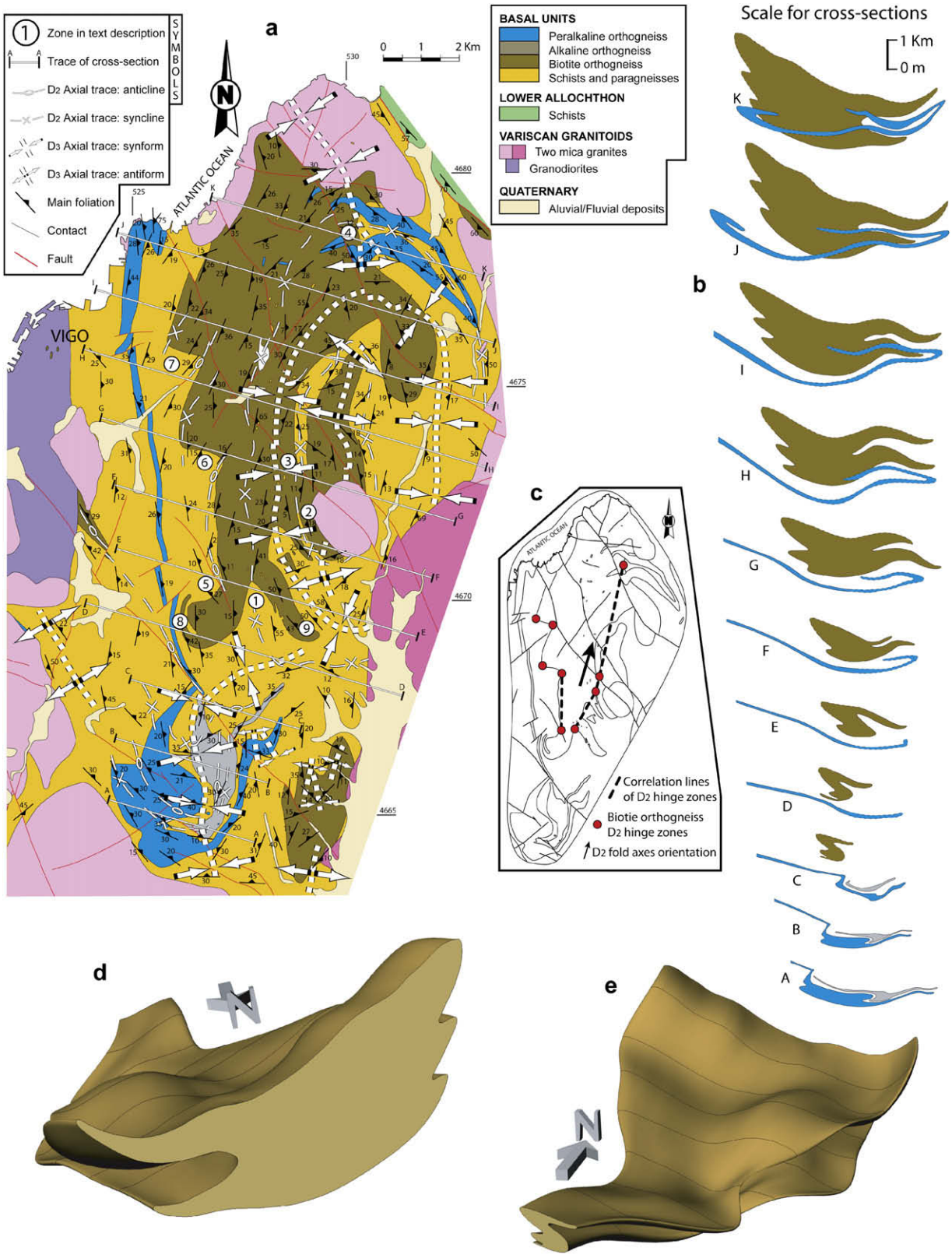

Fig. 10. (a) Structural map showing D_2 and D_3 axial traces. (b) Serial cross-sections drawn normal to the mean D_2 fold axis. (c) Sketch with the correlation of D_2 hinge zones (thick dashed lines) that support a NE to NNE trend for D_2 folds. Fault displacements have been removed in the cross-sections to obtain the clearest vision possible of the ductile structures. Numbers 1 to 9 on the map indicate zones described in the text. Dashed lines in the sections indicate interpretation not constrained by the map. (d, e) Two 3D perspectives of the main massif of biotite orthogneiss made tracing a surface envelope joining the structurally correlated and regularly spaced cross-sections in (b). The sections can be recognized as thin lines on the surface of the model (sections D– J) or as flat surfaces at model ends (sections C and K).

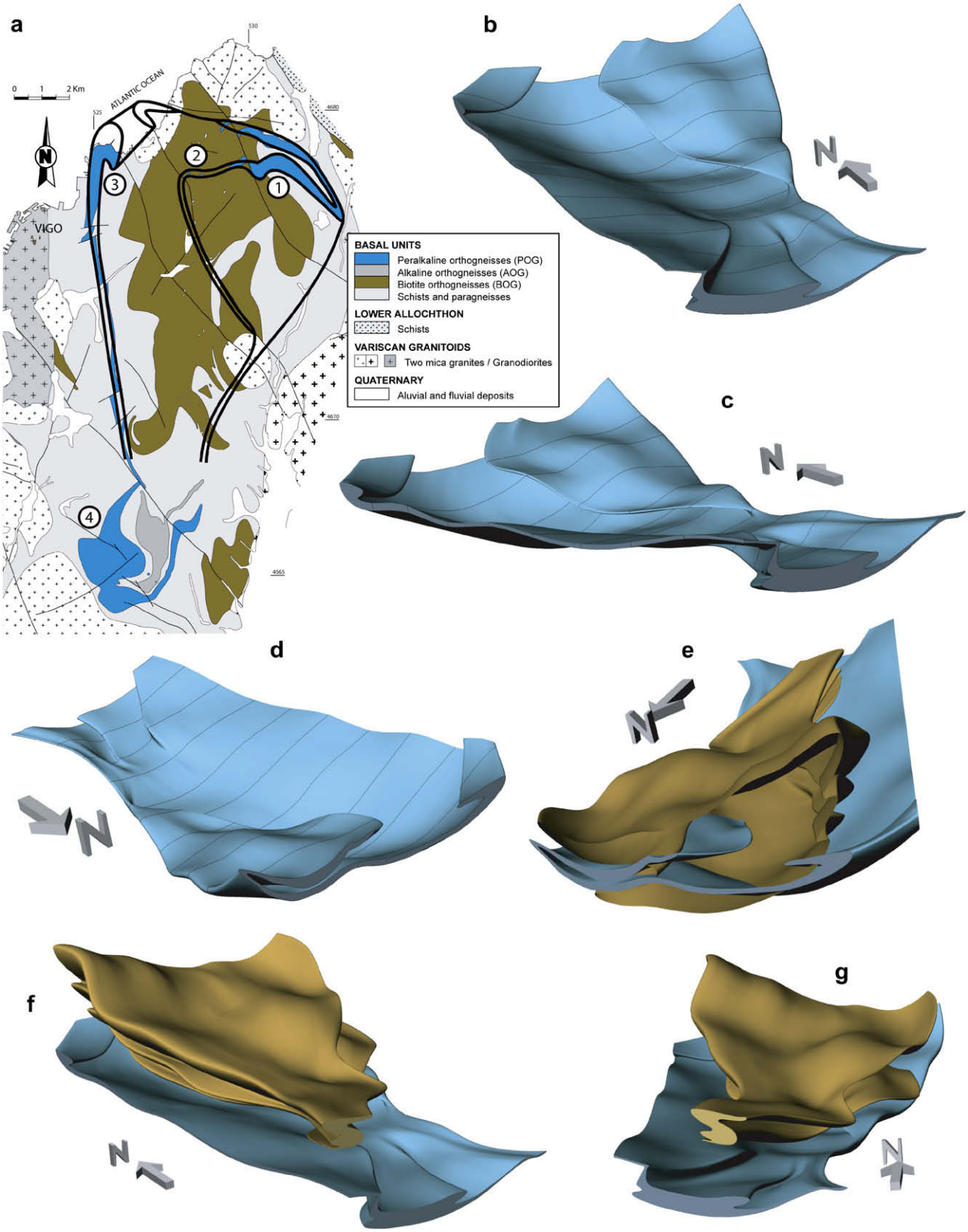

Fig. 11. (a) Interpretation of the peralkaline orthogneiss as a single body, sketched with a thick black line, which includes the tight fold-like structure in the northeast (1), the isolated masses cropping out to the west of it (2), the elongated band ending with an inflexion in the northwest (3), and the recumbent train of folds in the south (4). (b–d) 3D perspectives of the peralkaline orthogneiss interpreted as a single pluton. Its shape may represent an incomplete ring dike flattened and stretched. Thin lines and model ends show the cross-sections A– K of Fig. 10b. (e–g) Fusion of the models of the peralkaline and biotite orthogneisses to give a full vision of the 3D structure. The biotite orthogneiss is shown hollow in (e) to reveal its inner parts and how both plutons interfere with each other.

igneous mass pinches out quickly toward the north, pointing also in this case to a lenticular shape elongated in the N–S direction and affected by the recumbent folds (Figs. 7 and 10b).

The combination of 3D models made for both gneiss bodies shows a realistic view of the structure in the southern part of the Malpica–Tui Unit (Fig. 11e–g). Their superposition permits to see how both plutons are elongated subparallel to the mean direction of the L_2 stretching lineation (344°/12° in the southernmost part, with a mean of 345°/3° for the whole area using the mean values of the different domains of Fig. 4). Cross-cutting relationships between both plutons are ambiguous, and not clear enough to establish their relative order of intrusion. However, a younger age of the peralkaline and alkaline orthogneisses can be deduced from deformed mafic dikes, presently represented by amphibolite lenses, which are common in the biotite orthogneisses and the metasediments, but absent in the alkaline and peralkaline orthogneisses.

5. Relationships between composition and shape of the plutons

Once the general structure of the more representative orthogneisses has been established, it is possible to interpret their shape singularities, especially when the emplacement morphology could be strongly conditioned by the stress regime, previous structures and available room during their intrusion.

The extension of a stable continental margin or the break-up of the continental lithosphere during intracontinental rifting may imprint a geochemical, petrological and structural signature on the associated magmas. In this geodynamic context, alkaline magmatism, emplacement at shallow levels, and the annular geometry of plutons, intruded in conical faults during extension are common (Anderson, 1936; Lipman, 1997; Bonin, 2007; Gudmundsson, 2007).

Petrologic and geochemical studies of the igneous rocks of the Malpica–Tui Unit (Floor, 1966; Ribeiro and Floor, 1987; Corretgé et al., 1990; Pin et al., 1992; Montero, 1993; Rodríguez Aller, 2005) have classified the peralkaline and alkaline gneisses as A-type anorogenic alkaline granitoids (Whalen et al., 1987; Eby, 1990) with a strong mantelic affinity and generated in an intraplate context during Ordovician continental rifting.

Alkaline magmatism has been classically related with extensional geodynamic contexts, in which thinning and depressurization of the base of the crust and the upper mantle generate alkaline melts that activate volcano-plutonic plumbing systems. A complete system includes plutons below and volcanic cauldrons above (Cole et al., 2005 and references therein), with annular subvolcanic complexes between them as representatives of the magma pathways from the deeper to the shallower levels (Lipman, 1984 and references therein).

Differential erosive dismantlement of recent alkaline complexes makes it possible to study their different structural levels. Many granitoids and subvolcanic rocks related with the extensional process depict an oval to circular pattern in map view and the shape of the frustum of a cone in 3D, with the walls dipping either inward or outward. These are known as ring dikes (Johnson et al., 2002), and their shape is a consequence of faulting by overpressure in the chamber (Phillips, 1974), followed by fracturing and subsequent collapse of the roof above the magma chamber because of degasification and magma loss. The diameter of ring dikes may vary from less than two kilometres (Johnson et al., 2002) to several tens of kilometres (Peucat et al., 2005).

These facts about alkaline magmatism provide an interpretation for the semiannular structure of the peralkaline gneiss hosted in the core of the D_2 syncline folding the biotite gneiss (Figs. 10 and 11), which could result from the flattening and stretching of an incomplete ring dike.

6. Structural evolution

The intrusion of pre-Variscan granitoids took place in the Malpica–Tui Unit during the Early to Middle Ordovician, with ages ranging between 490 and 460 Ma (Priem et al., 1966; Van Calsteren et al., 1979; García Garzón et al., 1981; Montero et al., 1998; Santos Zalduegui et al., 1995; Rodríguez et al., 2003, 2007). The mantle-related geochemistry of the alkaline and peralkaline plutons (Pin et al., 1992; Montero, 1993; Rodríguez Aller, 2005) and the structural evidences of crustal extension in NW Iberia during the Ordovician (Martínez Catalán et al., 1992), depict a rifting scenario for northern Gondwana.

At a given stage of evolution, after the intrusion of the biotite granitoids of calc-alkaline affinity, basic dikes intruded, that are now preserved as boudins in the orthogneisses and metasediments. The emplacement of alkaline and peralkaline magmas corresponds to the last recognizable magmatic stages. Since for alkaline magmas in rift contexts, kilometre-scale plutons with circular, oval, arcuate, or polygonal shapes in plan view can be expected, we will now consider if the fold-like structure in the northeast of the peralkaline gneiss (Fig. 11a–d) can be a ring dike. It would represent an incomplete frustum of a cone in any case, as the pluton pinches out in the southeast and its map pattern is not a fully closed form.

The alternative possibility is a sheath fold affecting a sheet-like pluton. Sheath folds may develop either by inhomogeneous flow or by amplification of initially curved fold hinges in ductile shear zones characterized by large simple shear strain (Cobbold and Quinquis, 1980; Ramsay and Huber, 1987). Continuity in the curved hinge zone should be expected, at least in the case of the latter mechanism, because the apical structure is a feature inherent to sheath fold development. In our case, the lack of continuity in the peralkaline orthogneiss in the western half of the supposed apical zone (area 2 in Fig. 11a) does not support the sheath fold hypothesis. Moreover, the apical direction of the supposed sheath fold would be NNE–SSW to NE–SW, which does not fit the mean value of the mineral and stretching lineation (345°/3°).

The possibility that the semiannular form of the peralkaline orthogneiss is a fold developed together with the NNE–SSW recumbent syncline in the biotite orthogneiss, starting from two mutually oblique plutons, cannot be ruled out, but the final folded shape of the peralkaline orthogneiss would be favoured if it was initially arcuate instead of planar, as primary curvature could have nucleated the sheath fold.

Notwithstanding, it is the peralkaline composition and the common association of this type of rocks with ring dikes that favour our hypothesis of the peralkaline gneiss as derived from an incomplete ring dike. Fig. 12 demonstrates that the ring dike option is geometrically feasible. It shows how a curved sheet representing the incomplete frustum of a cone which intersects a massive pluton (Fig. 12a) is deformed by superimposed general shear (Fig. 12b) and once both plutons had been strongly flattened and stretched, are affected by recumbent folding (Fig. 12c).

Actually, Fig. 12 has been built just in the opposite direction, from c to a, starting from the sections of Fig. 10b. We have assimilated every section of the peralkaline and biotite orthogneisses to ellipses and unstrained them homogeneously in order to remove the strain undergone during D_1 and D_2. In the case of the peralkaline orthogneiss, all ellipses have the same aspect ratio, parallel axes and a size proportional to their distance to section K of Fig. 10b, which is the smallest one. The aim is to obtain a perfect frustum of a cone after unstraining. For the biotite orthogneiss, the initial

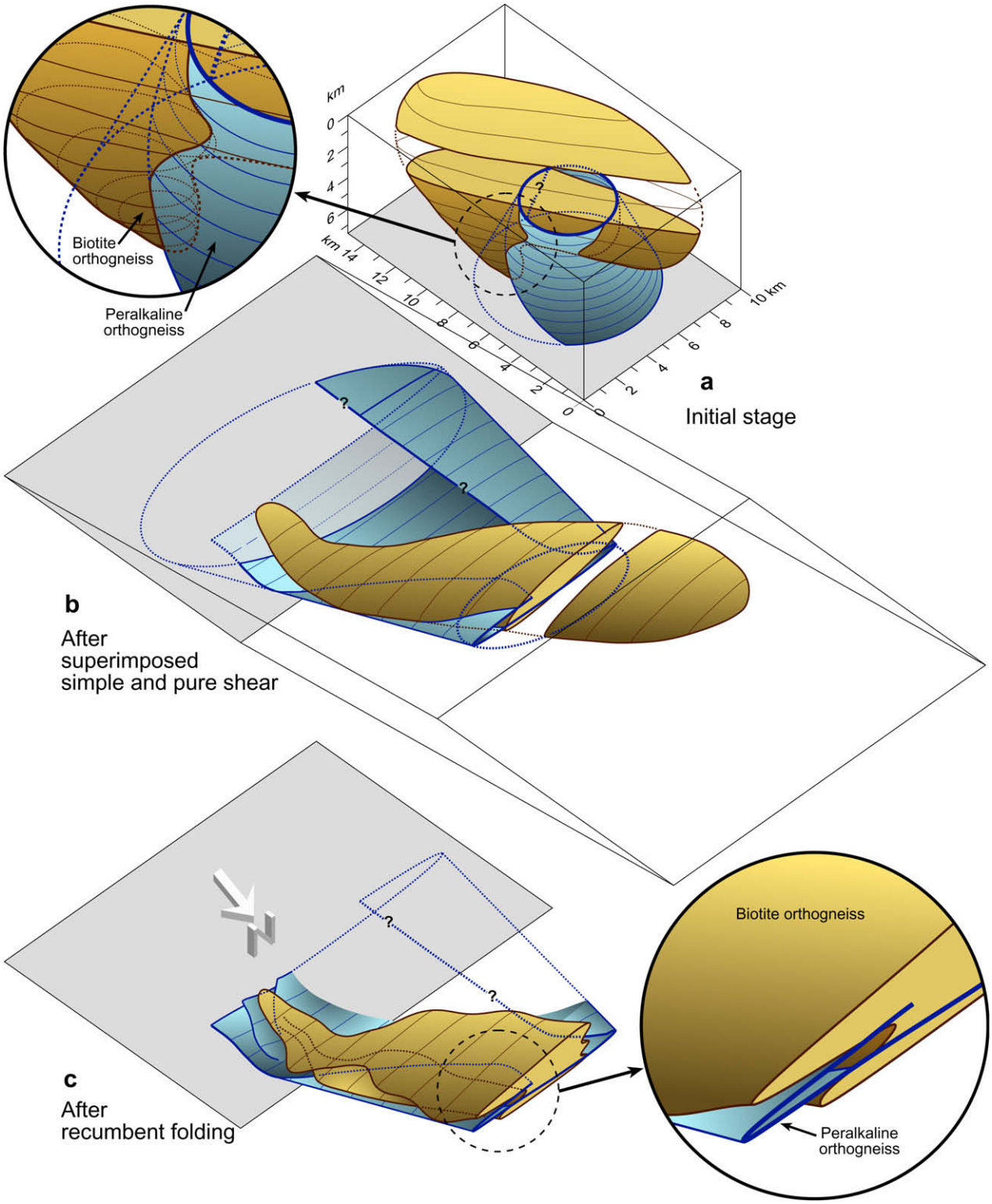

Fig. 12. (a) Proposed initial geometry and mutual relationships between the main massifs of peralkaline and biotite orthogneisses in the south of the Malpica–Tui Unit. The peralkaline orthogneiss is idealized as a curved sheet representing the incomplete frustum of a cone, and intersecting the biotite orthogneiss, a massive ovoid pluton rooting inside the cone (inset). Subsequent evolution shows homogeneous deformation by superimposed general shear (b) and recumbent folding (c). The inset in (c) shows the core of the recumbent syncline in the biotite orthogneiss hosting what is apparently a recumbent anticline but in fact may represent the eastern edge of the flattened cone. Question marks indicate that while the eastern edge of the peralkaline orthogneiss is reasonably well constrained by the outcrop pattern, its geometry in the western side is not, because erosion has removed what might represent a substantial part of the pluton.

ellipses had different size and orientation, and were drawn with the relative inclination and position with respect to the peralkaline orthogneiss shown in the lower limb of the recumbent syncline in the sections of Fig. 10b. In the subsequent unstraining process, the regular elliptical form of the biotite orthogneiss ellipses was modified somewhat to obtain an undeformed pluton free from small irregularities.

The assimilation of the sections to ellipses is equivalent to removal of the effects of upright and recumbent folding. Unstraining was accomplished by superposition of homogeneous pure shear followed by simple shear, in such a way as to transform the flattened frustum of a cone of Fig. 12b to that of a perfect cone with an apical angle close to 50° (Fig. 12a). There are many uncertainties in the actual form of the original sections, and the strain values are arbitrary, as there are no available strain markers. So, the cone must be regarded as an idealized target representing the starting pluton shape. That geometry explains the semiannular fold-like structure of the peralkaline orthogneiss in the core of the recumbent syncline in the biotite gneiss (zone 4 in Fig. 10a) as one of the edges of the extremely flattened cone (inset in Fig. 12c). Furthermore, providing that the geometry of the peralkaline pluton was that of the frustum of a cone, the biotite-rich pluton would have shown an initial ovoid shape with a root zone, probably the feeding conduit, part of which would have been included inside the cone (inset in Fig. 12a).

7. Conclusions

The structural study of three orthogneiss massifs of different compositions in the southern part of the Malpica–Tui Unit demonstrates that they are folded by a generation of recumbent folds with associated axial planar foliation and mineral lineation. These fabrics are exhumational, and represent the second deformation event, after a first one developed under high-pressure conditions. The whole deformation history includes subduction, exhumation along a continental-scale shear zone where the recumbent folds developed, and late extension during late orogenic collapse, plus upright open folding.

The structural analysis shows that the two largest massifs, peralkaline and biotite orthogneisses respectively, are elongated in the N–S direction, subparallel to the mineral lineation, and affected by recumbent folds with east vergence and axes varying from N–S to NE–SW. A large recumbent syncline folds the biotite orthogneiss whereas a train of asymmetric folds developed in the southern part of the peralkaline orthogneiss in what corresponds to the normal limb of the recumbent syncline. A small massif of alkaline orthogneiss is also folded by the train of asymmetric folds in the southern part.

The geometry of the folds has been accurately deduced using down-plunge projections and is constrained by the fact that two of the fold hinges crop out more than once due to late folding. A series of regularly spaced cross-sections has been used to build a three-dimensional model of the two main orthogneisses showing their folded geometry and mutual relationships. The peculiar geometry of the peralkaline orthogneiss is viewed as inherited from its primary shape, and is interpreted as a ring dike, in accordance with the common association of this geometry with igneous bodies of the alkaline suite, and because it probes to be geometrically feasible.

Our study demonstrates that detailed mapping and structural analysis can be used to identify and characterize superimposed folds in orthogneiss massifs and to construct 2D and 3D models of their present geometry. This in turn may be used to show their mutual geometric relationships and envisage their original shape.

Acknowledgements

We thank Dr. R. Arenas and Dr. J. Abati for their crucial help and comments on the petrographic analyses of the schists and gneisses. This work has been funded by the projects CGL2004-04306-C02/BTE and CGL2007-65338-C02/BTE of the Spanish Ministerio de Educación y Ciencia. It is also a contribution to the Project IGCP 497: The Rheic Ocean: Its Origin, Evolution and Correlatives. Jürgen von Raumer and an anonymous referee are acknowledged for their positive evaluation and a careful revision of the manuscript.

References

Abati, J., Arenas, R., Martínez Catalán, J.R., Díaz García, F., 2003. Anticlockwise P-T path of granulites from the Monte Castelo Gabbro (Órdenes Complex, NW Spain). Journal of Petrology 44, 305–327.

Anderson, E.M., 1936. The dynamics of the formation of cone-sheets, ring dykes, and cauldron-subsidence. Proceedings of the Royal Society of Edinburgh 56, 128–163.

Andonaegui, P., González del Tánago, J., Arenas, R., Abati, J., Martínez Catalán, J.R., Peinado, M., Díaz García, F., 2002. Tectonic setting of the Monte Castelo gabbro (Ordenes Complex, northwestern Iberian Massif): Evidence for an arc-related terrane in the hanging wall to the Variscan suture. In: Martínez Catalán, J.R., Hatcher Jr., R.D., Arenas, R., Díaz García, F. (Eds.), Variscan-Appalachian Dynamics: the Building of the Late Paleozoic Basement. Geological Society of America Special Paper, 364, pp. 37–56.

Aranguren, A., Cuevas, J., Tubía, J.M., Román-Berdiel, T., Casas-Sáinz, A., Casas-Ponsati, A., 2003. Granite laccolith emplacement in the Iberian arc: AMS and gravity study of the La Tojiza pluton (NW Spain). Journal of the Geological Society London 160, 435–445.

Arenas, R., Rubio Pascual, F.J., Díaz García, F., Martínez Catalán, J.R., 1995. High-pressure micro-inclusions and development of an inverted metamorphic gradient in the Santiago Schists (Ordenes Complex, NW Iberian Massif, Spain): evidence of subduction and syn-collisional decompression. Journal of Metamorphic Geology 13, 141–164.

Arenas, R., Martínez Catalán, J.R., Sánchez Martínez, S., Fernández-Suárez, J., Andonaegui, P., Pearce, J.A., Corfu, F., 2007. The Vila de Cruces Ophiolite: A remnant of the early Rheic Ocean in the Variscan suture of Galicia (NW Iberian Massif). Journal of Geology 115, 129–148.

Barbarin, B., 1999. A review of the relationships between granitoid types, their origins and their geodynamic environments. Lithos 46, 605–626.

Bonin, B., 2007. A-type granites and related rocks: Evolution of a concept, problems and prospects. Lithos 97, 1–29.

Bouchez, J.L., Gleizes, G., Djouadi, T., Rochette, P., 1990. Microstructure and magnetic susceptibility applied to emplacement kinematics of granites: the example of the Foix pluton (French Pyrenees). Tectonophysics 184, 157–171.

Bozkurt, E., Park, R.G., 1997. Microstructures of deformed grains in the augen gneisses of southern Menderes Massif and their tectonic significance. Geologische Rundschau 86, 103–119.

Cobbold, P.R., 1975. Fold propagation in single embedded layers. Tectonophysics 27, 333–351.

Cobbold, P.R., Quinquis, H., 1980. Development of sheath folds in shear regimes. Journal of Structural Geology 2, 119–126.

Cole, J.W., Milner, D.M., Spinks, K.D., 2005. Calderas and caldera structures: a review. Earth-Science Reviews 69, 1–26.

Corretgé, L.G., Rambaud, F., González Montero, P., Villa, L., Suárez, O., 1990. Petrología y geoquímica de los ortoneises alcalinos del Monte Galiñeiro (Provincia de Pontevedra). Boletín de la Sociedad Española de Mineralogía 13 (1), 136.

Coward, M.P., 1972. The structure and origin of areas of anomalously low-intensity finite deformation in the basement gneiss complex of the Outer Hebrides. Tectonophysics 16, 117–140.

Díaz García, F., 1990. La geología del sector occidental del Complejo de Ordenes (Cordillera Hercínica, NW de España). In: Serie Nova Terra, 3. Laboratorio Xeolóxico de Laxe. 230pp.

Díaz García, F., Arenas, R., Martínez Catalán, J.R., González del Tánago, J., Dunning, G., 1999. Tectonic evolution of the Careón ophiolite (Northwest Spain): a remnant of oceanic lithosphere in the Variscan belt. Journal of Geology 107, 587–605.

Eby, G.N., 1990. The A-Type granitoids: A review of their occurrence and chemical characteristics and speculations on their petrogenesis. Lithos 26, 115–134.

Floor, P., 1966. Petrology of an aegirine-ribeckite gneiss-bearing part of the Hesperian Massif: The Galiñeiro and surrounding areas, Vigo, Spain. Leidse Geologische Mededelingen 36, 1–204.

García Garzón, J., Pablo Maciá, J.G., Llamas Borrajo, J.F., 1981. Edades absolutas obtenidas mediante el método Rb-Sr de dos cuerpos de ortogneises en Galicia Occidental. Boletín Geológico y Minero 92, 443–455.

Gil Ibarguchi, J.I., Ortega Gironés, E., 1985. Petrology, structure and geotectonic implications of glaucophane-bearing eclogites and related rocks from the Malpica-Tuy (MT) Unit, Galicia, Northwest Spain. Chemical Geology 50, 145–162.

Gudmundsson, A., 2007. Conceptual and numerical models of ring-fault formation. Journal of Volcanology and Geothermal Research 164, 142–160.

Higashino, T., 1990. The higher grade metamorphic zonation of the Sanbagawa metamorphic belt in central Shikoku, Japan. Journal of Metamorphic Geology 8, 413–423.
Holdaway, M.J., 1971. Stability of andalusite and the aluminium silicate phase diagram. American Journal of Science 271, 97–131.
Iglesias Ponce de León, M., Choukroune, P., 1980. Shear zones in the Iberian arc. Journal of Structural Geology 2, 63–68.
Johnson, S.E., Schmidt, K.L., Tate, M.C., 2002. Ring complexes in the Peninsular Ranges Batholith, Mexico and the USA: magma plumbing systems in the middle and upper crust. Lithos 61, 187–208.
Lipman, P.W., 1984. The roots of ash-flow calderas in North America: windows into the tops of granitic batholiths. Journal of Geophysical Research 89, 8801–8841.
Lipman, P.W., 1997. Subsidence of ash-flow calderas: relation to caldera size and magma chamber geometry. Bulletin of Volcanology 59, 198–218.
Mackin, J.H., 1950. The down-structure method of viewing geologic maps. Journal of Geology 58, 55–72.
Martínez Catalán, J.R., Hacar Rodríguez, M.P., Villar Alonso, P., Pérez-Estaún, A., González Lodeiro, F., 1992. Lower Paleozoic extensional tectonics in the limit between the West Asturian-Leonese and Central Iberian Zones of the Variscan Fold-Belt in NW Spain. Geologische Rundschau 81, 545–560.
Martínez Catalán, J.R., Arenas, R., Díaz García, F., Rubio Pascual, F.J., Abati, J., Marquínez, J., 1996. Variscan exhumation of a subducted Paleozoic continental margin: The basal units of the Ordenes Complex, Galicia, NW Spain. Tectonics 15, 106–121.
Martínez Catalán, J.R., Arenas, R., Díaz García, F., Abati, J., 1997. Variscan accretionary complex of northwest Iberia: Terrane correlation and succession of tectonothermal events. Geology 25, 1103–1106.
Martínez Catalán, J.R., Arenas, R., Díaz García, F., Gómez-Barreiro, J., González Cuadra, P., Abati, J., Castiñeiras, P., Fernández-Suárez, J., Sánchez Martínez, S., Andonaegui, P., Gónzalez Clavijo, E., Díez Montes, A., Rubio Pascual, F.J., Valle Aguado, B., 2007. Space and time in the tectonic evolution of the northwestern Iberian Massif. Implications for the Variscan belt. In: Hatcher Jr., R.D., Carlson, M.P., McBride, J.H., Martínez Catalán, J.R. (Eds.), 4-D framework of continental crust. Geological Society of America Memoir, 200, pp. 403–423.
Martínez Catalán, J.R., Fernández-Suárez, J., Meireles, C., González Clavijo, E., Belousova, E., Saeed, A., 2008. U–Pb detrital zircon ages in synorogenic deposits of the NW Iberian Massif (Variscan belt): interplay of Devonian-Carboniferous sedimentation and thrust tectonics. Journal of the Geological Society, London 165, 687–698.
Montero, P., 1993. Geoquímica y petrogénesis del Complejo Peralcalino de la Sierra del Galiñeiro (Pontevedra, España). Ph.D. thesis, University of Oviedo.
Montero, P., Floor, P., Corretgé, L.G., 1998. The accumulation of rare-earth and high-field-strength elements in peralkaline granitic rocks: the Galiñeiro orthogneissic complex, Northwestern Spain. Canadian Mineralogist 36, 683–700.
Munhá, J., Ribeiro, A., Ribeiro, M.L., 1984. Blueschists in the Iberian Variscan Chain (Trás-os-Montes: NE Portugal). Comunicações dos Serviços Geológicos de Portugal 70, 31–53.
Neves, S.P., Araújo, A.M.B., Correia, P.B., Mariano, G., 2003. Magnetic fabrics in the Cabanas Granite (NE Brazil): interplay between emplacement and regional fabrics in a dextral transpressive regime. Journal of Structural Geology 25, 441–453.
Otsuki, M., Banno, S., 1990. Prograde and retrograde metamorphism of haematite-bearing basic schists in the Sanbagawa belt in central Shikoku. Journal of Metamorphic Geology 8, 425–439.
Peucat, J.-J., Capdevila, R., Drareni, A., Mahdjoub, Y., Kahoui, M., 2005. The Eglab massif in the West African Craton (Algeria), an original segment of the Eburnean orogenic belt: petrology, geochemistry and geochronology. Precambrian Research 13, 309–352.
Phillips, W.S., 1974. The dynamic emplacement of cone sheets. Tectonophysics 24, 69–84.
Pin, C., Ortega Cuesta, L.A., Gil Ibarguchi, J.I., 1992. Mantle-derived, early Paleozoic A-type metagranitoids from the NW Iberian Massif: Nd isotope and trace-element constraints. Bulletin de la Societé Géologique de France 163, 483–494.
Pin, C., Paquette, J.L., Santos Zalduegui, J.F., Gil Ibarguchi, J.I., 2002. Early Devonian supra-subduction zone ophiolite related to incipient collisional processes in the Western Variscan Belt: The Sierra de Careón unit, Ordenes Complex, Galicia. In: Martínez Catalán, J.R., Hatcher, R.D., Arenas, R., Díaz García, F. (Eds.), Variscan-Appalachian Dynamics: the Building of the Late Paleozoic Basement. Geological Society of America Special Paper, 364, pp. 57–72.
Pin, C., Paquette, J.L., Ábalos, B., Santos, F.J., Gil Ibarguchi, J.I., 2006. Composite origin of an early Variscan transported suture: Ophiolitic units of the Morais Nappe Complex (north Portugal). Tectonics 25, TC5001, doi:10.1029/2006TC001971.
Pitcher, W.S., 1993. The Nature and Origin of Granite. Blackie Academic & Professional, London, 321 pp.
Priem, H.N.A., Boelrijk, N.A.I.M., Verschure, R.H., Hebeda, E.H., Floor, P., 1966. Isotopic evidence for Upper-Cambrian or Lower-Ordovician granite emplacement in the Vigo Area, North-Western Spain. Geologie en Mijnbouw 45, 36–40.
Ramsay, J.G., 1967. Folding and Fracturing of Rocks. McGraw-Hill, New York, 590 pp.
Ramsay, J.G., Huber, M.I., 1987. Modern Structural Geology. In: Folds and Fractures, Vol. 2. Academic Press, London, pp. 309-700.
Ribeiro, M.L., Floor, P., 1987. Magmatismo peralcalino no Maciço Hespérico: sua distribução e significado geodinámico. In: Bea, F., Carnicero, A., Gonzalo, J.C., López-Plaza, M., Rodríguez Alonso, M.D. (Eds.), Geología de los granitoides y rocas asociadas del Macizo Hespérico. Rueda, Madrid, pp. 211–221.
Rodríguez Aller, J., 2005. Recristalización y deformación de litologías supracorticales sometidas a metamorfismo de alta presión (Complejo de Malpica-Tuy, NO del Macizo Ibérico). In: Nova Terra, 29. Laboratorio Xeolóxico de Laxe. 572pp.
Rodríguez, J., Cosca, M.A., Gil Ibarguchi, J.I., Dallmeyer, R.D., 2003. Strain partitioning and preservation of $^{40}Ar/^{39}Ar$ ages during Variscan exhumation of a subducted crust (Malpica–Tui complex, NW Spain). Lithos 70, 111–139.
Rodríguez, J., Paquette, J.L., Gil Ibarguchi, J.I., 2007. U-Pb dating of Lower Ordovician alkaline magmatism in the Gondwana margin (Malpica–Tui complex, Iberian Massif): latest continental events before oceanic spreading. In: Arenas, R., Martínez Catalán, J.R., Abati, J., Sánchez Martínez, S. (Eds.), IGCP 497: The Rheic Ocean—Its Origin, Evolution and Correlatives, A Coruña, Spain, The Rootless Variscan suture of NW Iberia (Galicia, Spain), Field trip guide & Conference abstracts, pp. 163–164.
Rubio Pascual, F.J., Arenas, R., Díaz García, F., Martínez Catalán, J.R., Abati, J., 2002. Eclogites and eclogite-amphibolites from the Santiago Unit (Ordenes Complex, NW Iberian Massif, Spain): a case study of contrasting high-pressure metabasites in a context of crustal subduction. In: Martínez Catalán, J.R., Hatcher, R.D., Arenas, R., Díaz García, F. (Eds.), Variscan–Appalachian Dynamics: The Building of the Late Paleozoic Basement. Geological Society of America Special Paper, 364, pp. 105–124.
Sánchez Martínez, S., Arenas, R., Díaz García, F., Martínez Catalán, J.R., Gómez-Barreiro, J., Pearce, J.A., 2007. Careón Ophiolite, NW Spain: Suprasubduction zone setting for the youngest Rheic Ocean floor. Geology 35, 53–56.
Santos, J.F., Schärer, U., Gil Ibarguchi, J.I., Girardeau, J., 2002. Genesis of pyroxenite-rich peridotite at Cabo Ortegal (NW Spain): geochemical and Pb-Sr-Nd isotope data. Journal of Petrology 43, 17–43.
Santos Zalduegui, J.F., Schärer, U., Gil Ibarguchi, J.I., 1995. Isotope constraints on the age and origin of magmatism and metamorphism in the Malpica-Tuy allochthon, Galicia, NW-Spain. Chemical Geology 121, 91–103.
Schermerhorn, L.J.G., Kotsch, S., 1984. First occurrence of lawsonite in Portugal and tectonic implications. Comunicações dos Serviços Geológicos de Portugal 70, 23–29.
Simancas, J.F., Galindo-Zaldívar, J., Azor, A., 2000. Three-dimensional shape and emplacement of the Cardenchosa deformed pluton (Variscan Orogen, southwestern Iberian Massif). Journal of Structural Geology 22, 489–503.
Takasu, A., Dallmeyer, R.D., 1990. $^{40}Ar/^{39}Ar$ mineral age constraints for the tectonothermal evolution of the Sanbagawa metamorphic belt, central Shikoku, Japan: a Cretaceous accretionary prism. Tectonophysics 185, 111–139.
Talbot, J.Y., Martelet, G., Courrioux, G., Chen, Y., Faure, M., 2004. Emplacement in an extensional setting of the Mont Lozère-Borne granitic complex (SE France) inferred from comprehensive AMS, structural and gravity studies. Journal of Structural Geology 26, 11–28.
Talbot, J.Y., Faure, M., Chen, Y., Martelet, G., 2005. Pull-apart emplacement of the Margeride granitic complex (French Massif Central). Implications for the late evolution of the Variscan orogen. Journal of Structural Geology 27, 1610–1629.
Tullis, J., Yund, R.C., 1985. Dynamic recrystallization of feldspar: a mechanism for ductile shear zone formation. Geology 13, 238–241.
Vacas Peña, J.M., 2001. Isogons: a program in Pascal to draw the dip isogons of folds. Computers & Geosciences 27, 601–606.
Van Calsteren, P.W.C., Boelrijk, N.A.I.M., Hebeda, E.H., Priem, H.N.A., Tex, E., Den, Verdurmen, E.A.T.H., Verschure, R.H., 1979. Isotopic dating of older elements (including the Cabo Ortegal mafic-ultramafic complex) in the Hercynian Orogen of NW Spain: manifestations of a presumed Early Paleozoic Mantle-plume. Chemical Geology 24, 35–56.
Watterson, J., 1968. Homogeneous deformation of the gneisses of Vesterland, southwest Greenland. Gronlands Geologiske Undersogelse Bulletin 78, 75.
Whalen, J.B., Currie, K.L., Chappell, B.W., 1987. A-Type granites: geochemical characteristics, discrimination and petrogenesis. Contributions to Mineralogy and Petrology 95, 407–419.
Yenes, M., Álvarez, F., Gutiérrez-Alonso, G., 1999. Granite emplacement in orogenic compressional conditions: the La Alberca-Béjar granitic area (Spanish Central System, Variscan Iberian Belt). Journal of Structural Geology 21, 1419–1440.